Construction and Application of Transition Prediction Databased Method for 2 nd Mack Mode on Sharp Cone

Xavier Chanteux, Guillaume Bégou, Hugues Deniau, Olivier Vermeersch

Construction and Application of Transition Prediction Databased Method for 2nd Mack Mode on Sharp Cone

Xavier Chanteux * and Guillaume Bégou †
DAAA, ONERA, Université Paris Saclay, F-92190 Meudon - France

Hugues Deniau‡ and Olivier Vermeersch§
ONERA-The French Aerospace Lab, Toulouse, France

This study investigates the development of a Reynolds-averaged Navier–Stokes (RANS) model for natural laminar-turbulent transition based on local linear stability theory (LST), and its ability to predict growth rate evolution of Mack's second mode. Unstable growth rates for a given frequency are derived from analytical relations for which coefficients are stored in a database. The beginning of the transitional region is then obtained from the e^N-method which consists in integrating the disturbance growth rates along its path of amplification. This approach is an expansion of ONERA's parabolas method to hypersonic laminar-turbulent natural transition and is applied here on a 7° half-angle sharp cone at Mach 8.

Nomenclature

δ	=	Boundary layer thickness
δ_1	=	Boundary layer displacement thickness
θ	=	Boundary mayer momentum thickness
Re_{δ_1}	=	Reynolds number based on δ_1
Re_θ	=	Reynolds number based on θ
M_e	=	Mach number at boundary layer edge
k	=	Wavenumber vector
α	=	Longitudinal wavenumber
α_r	=	Real part of α
α_i	=	Imaginary part of α
β	=	Transversal wavenumber
β_r	=	Real part of β
ω	=	Angular frequency
f	=	Physical frequency
$\tilde{q}$	=	Amplitude of perturbations q
F	=	Reduced frequency
N	=	Amplification factor
M_∞	=	Free-stream Mach number
Re_∞	=	Free-stream Reynolds number
Ti_∞	=	Free-stream stagnation temperature
T_∞	=	Free-stream static temperature
Pi_∞	=	Free-stream stagnation pressure
s	=	Cone arclength

Introduction

BOUNDARY-LAYER laminar to turbulent transition is a critical factor in the design of hypersonic vehicles, such as reusable launch vehicles, high-speed interceptor missiles, hypersonic cruise or reentry vehicles: it affects all at once heat transfer, skin friction and boundary-layer properties [1]. Thus, it is of practical interest to use already available experiments and theory to evaluate transitional regions.

In this introduction, the term local refers to quantities accessible in each cell of the mesh, whereas non-local refers to quantities that need integration and/or searching algorithms. From an engineering point of view, Direct Numerical Simulations (DNS) and Large-Eddy Simulations (LES) can provide high-precision results and detailed flow field structures for transitional flows, yet are computationally expensive. With that in mind, efforts have been made to include transition phenomena in modern Reynolds-averaged Navier-Stokes (RANS) solvers *via* various methods that can roughly be sorted into two categories. On one hand, nonlocal methods based on the Linear Stability Theory (LST) , or Parabolized Stability Equations (PSE), combined with either meta-models [3] or databases [4] for physics-based applications, or coupled with RANS solvers. The transition onset then is determined by using the e^N-method ([5] and [6]). On the other hand, empirical transition criteria (C1 [7], AHD [8], Drela and Giles' [9] ...) used as is or as a basis for correlation-based transition models such as $\gamma - Re_\theta$ [10] model. This latter solution, originally designed by

*Ph.D. Candidate, Aerodynamics, Aeroelasticity, Aeroacoustic Department (DAAA-MASH)
†Research Engineer, Aerodynamics, Aeroelasticity, Aeroacoustic Department (DAAA-MASH)
‡Research Engineer, Aerodynamics and Energetics Modeling Department (DMPE-ITAC)
§Research Engineer, Aerodynamics and Energetics Modeling Department (DMPE-ITAC)

Menter and Langtry for turbomachine applications at low speed, uses local variables and transport equation for both intermittency and transition onset criteria, in order to evaluate a transition criteria from Re_θ, but includes no relevant physical phenomena. It has been extended to supersonic flows for scramjets by Frauholz et al. [11] and later to hypersonic flows by Wang et al. [12] using compressible similarity solutions.

Another local approach designed for turbomachine applications, using transport equations, is the $k_L - k_T - \omega$ model developed by Walters and Leylek [13] for bypass and natural transition, where k_L and k_T respectively describe the laminar and turbulent kinetic energy. On the other hand, Warren and Hassan [14] developed a nonlocal method based on LST results, using the time scale of instabilities and taking the contribution of the nonturbulent fluctuations into account. In 2016, inspired by the work of Walter and Leylek, Xu et al. [15] established a fully local transition closure model by combining all together Warren and Hassan's modeling idea, incorporating the transport equations for laminar and transitional solutions of Papp and Dash [16], with Menter and Langtry's model for intermittency. It was extended to hypersonic transitional flows dominated by the first and second mode, and laminar separation in 2017 [17]. Wang and Fu [18] and Wang and Fu [19] also combined these models between 2009 and 2012 to design their $k - \omega - \gamma$ local model for hypersonic transitional flows, which was improved recently by Zhou et al. ([20], [21], [22]).

Although all these methods give sufficient results very quickly, they are usually not reliable over a wide range of flow conditions because of the significant number of parameters influencing transition, and give no insight into its mechanism [23]. Comprehensive physics-based methods are therefore required in RANS solvers, and this means that, at some point, flow stability must be considered either with LST for slightly nonparallel flows, or PSE to account for nonparallel effects. These two methods consider perturbation amplitudes to grow linearly, and estimate the amplification rate for a given base flow, at a specified frequency. However, they do not acount for nonlinear interactions. Amplification rates are usually stored in some database, and the transition onset is evaluated using the e^N-method developed in 1956 independently by Van Ingen [5] and Smith and Gamberoni [6]: it consists, for a given mode (frequency and amplification direction), in integrating the growth rate along its path of amplification. Later, Van Ingen [24] built a database containing stability diagrams. Drela [25] also built one from stability results of self-similar profiles in order to take account for the varying incompressible shape factor H_i. In 1989, Arnal [4] used analytical relations to evaluate amplification rates evolution of self-similar profiles with respect to Reynolds number. The different coefficients are then tabulated with respect to some relevant flow parameters (integral thicknesses and M_e). This method is referred to as the parabolas method. It was first developed for two-dimensional incompressible flows over adiabatic walls Arnal [7], and extended to supersonic flows in 1995 by Arnal.

Databases can also be used to train metamodels. Fuller et al. [3] were the first ones to implement a neural network to predict growth rate in non reacting jet flows from frequency, wavenumber and momentum thickness. A few years later, Crouch et al. [26] developed a similar approach to predict Orr-Sommerfeld results for subsonic and transonic 3D swept-wing boundary layers. This model has been recently improved by Danvin et al. [27] for hypersonic flow.

These physics-based methods are often disparaged in the state of art because of the need to search and integrate non-local flow variables at the edge of boundary layers. In order to tackle this critic, Bégou et al. [28] recast the integration over a streamline into an advection equation with a source term. This solution allows to evaluate the amplification factor of the e^N-method by easily solving an additional transport equation. Combined with the parabolas method up to supersonic flows, this solution allows to evaluate the beginning of the transitional region. This new solution is called the NSP (N-σP) model.

This study focuses on extending the domain of application of the parabolas method to hypersonic flows by taking the evolution of the Mack mode into account.

I. Local Linear Stability Theory and Parabolas Method

A. Local Linear Stability Theory and e^N-Method

The linear stability theory, exposed in details by Mack [2], describes perturbations as normal modes propagating in a parallel (or slightly nonparallel) mean flow. The complete unsteady Navier-Stokes equations are linearized about the mean flow by writing each flow variable into a steady mean-flow term and an unsteady small disturbance term. Then the mean-flow solution is dropped from this set of equations, and cross products of disturbances are neglected (linear hypothesis) to obtain the disturbance equations. Mean-flow quantities are supposed to vary slowly in the longitudinal direction, allowing perturbations to be rewritten as normal modes

$$q = \tilde{q}(y)\ \mathbf{e}^{\mathbf{i}(\alpha x + \beta z - \omega t)} + \text{C.C.} \tag{1}$$

"C.C" denotes the complex conjugate that is needed for the disturbance field to remain real. In the most general case α, β, and ω are complex, but in this study β and ω are supposed real: the amplitude of the wave changes

as it propagates downstream in the x direction, which is called spatial amplification theory. The associated wavenumber k is defined by its amplitude $\mathrm{k} = \sqrt{\alpha_r^2 + \beta_r^2}$ and angular direction relative to the streamwise direction $\Psi = \tan^{-1}(\beta_r/\alpha_r)$. With the formulation of equation 1, the wave is amplified when α_i is negative. α can be extracted from the complete set of disturbance equations in order to write

$$\tilde{A}\,\tilde{\mathrm{q}} = \alpha \tilde{B}\,\tilde{\mathrm{q}}, \tag{2}$$

where $\tilde{\mathrm{q}} = \left(\tilde{\mathrm{u}}, \tilde{\mathrm{v}}, \tilde{\mathrm{w}}, \tilde{\mathrm{p}}, \tilde{\mathrm{T}}, \alpha\,\tilde{\mathrm{u}}, \alpha\,\tilde{\mathrm{v}}, \alpha\,\tilde{\mathrm{w}}, \alpha\,\tilde{\mathrm{T}}\right)^T$, and $\tilde{A}$ and $\tilde{B}$ are two $(9N \times 9N)$ matrices (where N is the total number of point of the discretization) containing the mean-flow quantities, and both their first and second derivatives with respect to the normal coordinate.

Solving this equation requires boundary conditions, which, for boundary layer flows, are defined as no-slip condition at wall surface $\tilde{\mathrm{q}}(0) = 0$, and no perturbation in the free-steam $\tilde{\mathrm{q}}\,(y \to \infty) = 0$. The set of boundary conditions and equation 2 define a general eigenvalue problem where α is the eigenvalue and $\tilde{\mathrm{q}}$ the eigenvector.

The linear local analyses are performed with an in-house stability code for ideal gas. Inspired by the work of Orszag [29], derivations are performed with a spectral method using Chebyshev polynomials, on the Gauss-Lobatto collocation points $y_j = \cos(\pi j/N)$ (with N being the total number of points in the collocation) recast such that half of the total number of points describe the boundary layer as suggested in Schmid and Henningson [30] (see Appendix A.5 on chebyshev discretization). Then, the eigenvalue problem is solved using geev function of LAPACK library.

In order to locate the beginning of the transitional region from LST, the $\mathrm{e^N}$-method is commonly used. It computes the amplification factor N of an instability, for a given reduced frequency F (see eq. 4), expressed as

$$\mathrm{N}(s,\,\mathrm{F}) = \ln\frac{A}{A_0} = \int_{s_{cr}}^{s} \sigma(\mathrm{F}, s)ds \tag{3}$$

where s is the path of amplification of $\sigma(\mathrm{F}, s)$, and s_{cr} the abscissa of the initial amplitude A_0 of the instability at the frequency F under consideration. This amplification factor can be regarded as a gain of energy of the disturbance as it propagates, and the transition is expected to occur for a critical value N_{tr}.

B. Parabolas Method for 1st Mode

In this section, all quantities are made dimensionless using $\mathrm{u_e}$ and δ_1.

When investigating the stability of (self-similar) profiles, stability diagrams are often plotted in the $(\mathrm{F}, Re_{\delta_1})$ coordinates, where F and Re_{δ_1} are defined by

$$\mathrm{F} = \frac{2\pi\ \mathrm{f}\nu_e}{\mathrm{u_e}^2} = \frac{\omega}{Re_{\delta_1}}, \quad Re_{\delta_1} = \frac{\rho_e\ \mathrm{u_e}\delta_1}{\mu_e} \tag{4}$$

Thus F evolves linearly with Re_{δ_1}: iso-values of F are lines with constant slope passing through the origin in the (ω, Re_{δ_1}) plan (see Fig. 2).

Arnal [4] observed that the evolution of the growth rate $\sigma = -\alpha_i$, for a given reduced frequency and plotted versus Re_{δ_1}, can be approximated by two half-parabolas for low speed flows. The equation yields, with Figure 1

$$\frac{\sigma}{\sigma_M} = 1 - \left[\frac{Re_{\delta_1} - R_M}{Re_k - R_M}\right]^2 \tag{5}$$

where

$$Re_k = \begin{cases} R_0 & Re_{\delta_1} < R_M \\ R_1 & Re_{\delta_1} > R_M \end{cases} \tag{6}$$

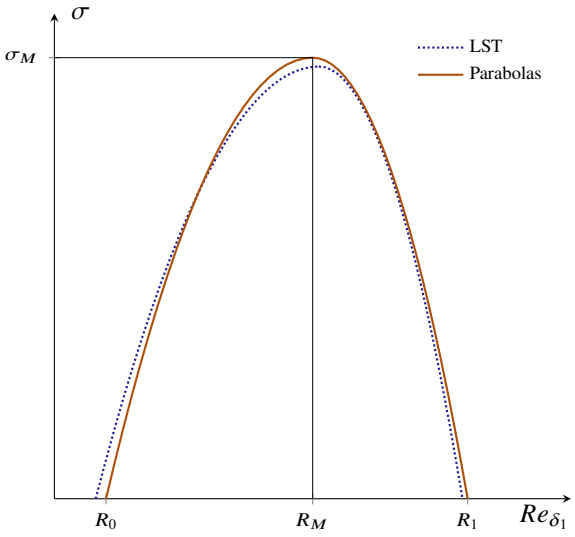

Figure 1: Qualitative comparison of LST and approximate growth rates (iso–F)

The parabolas parameters are then expressed as a function of the reduced frequency F

$$\sigma_M = A_M\left(1 - \frac{\mathrm{F}}{F_M}\right), \tag{7}$$

$$R_M = K_M\ \mathrm{F}^{E_M}, \tag{8}$$

$$R_0 = R_M\left[1 - A_0\left(1 - \frac{\mathrm{F}}{F_0}\right)\right], \tag{9}$$

$$R_1 = R_M\left[1 - A_1\left(1 - \frac{\mathrm{F}}{F_1}\right)\right]. \tag{10}$$

These new coefficients A_M, F_M, K_M, E_M, A_0, F_0, A_1 and F_1 are stored in a database indexed on the incompressible shape factor $\mathrm{H_i}$ and Mach number at boundary layer edge $\mathrm{M_e}$. Each point of the database corresponds

to the stability characteristics of the self-similar profile at specified (H_i, M_e), namely Falkner-Skan-Hartree profiles (which reduces to Blasius profiles in the abscence of pressure gradient) for incompressible flows, and Levy-Lees profiles for compressible ones.

This first model is called the viscous model and is designed for low-speed transitional flows in order to describe instabilities originating from viscous phenomena. Several corrections were added to this model to better describe new phenomena arising at higher velocities: instabilities may come from the presence of an inflection point in the mean profiles [31], which is taken into account through an additional dedicated set of two half-parabolas. A description of the complete parabolas method for the first mode is given in Bégou et al. [28].

II. Extension of Parabolas Method to 2nd Mode

In the following of previous studies on the parabolas method, the stability characteristics of Levy-Lees profiles are studied for the prediction of 2nd mode evolutions in unstable domains. To illustrate the construction method, an example for a baseflow (mean velocity and mean temperature profiles) at Mach number M_e=4.5 without any pressure gradient is shown here. The wall is set to adiabatic condition and Sutherland's viscosity law is used with a reference stagnation temperature at boundary-layer edge set to 300K.

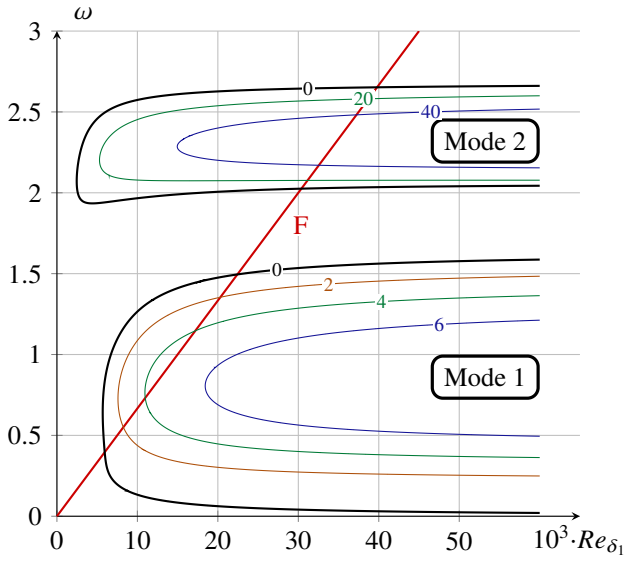

Figure 2: Stability Diagram at Mach 4.5: Contour lines $\alpha_i * 10^{-3}$

In the unstable domain of the 2nd mode, the amplification rate evolution σ (F, s) along a reduced frequency F - plotted in red in Figure 2 - is described with two half-parabolas and a linear correction to best fit the LST results. This linear correction is defined by matching first derivatives at $(\tilde{R}, \tilde{K}\sigma_M)$ (see Figure 3).

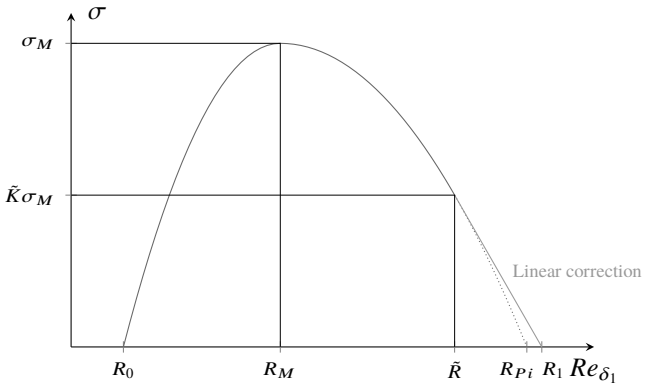

Figure 3: Definition of all parameters for two half-parabolas and linear correction (iso–F)

This modelization is optimized with a Sequential Least Squares Programming (SLSQP) algorithm. It minimizes, under constraints, the root-mean-squared error between the LST curve and the analytical model. Then, the evolution with F of each coefficient defining the model, namely R_0, R_M, $\tilde{R}$, R_1, and σ_M, are approximated with a correlation (see equations 11 - 15 and associated Figures 4 - 7), and each coefficient of these correlations - namely K_0, E_0, etc - are stored in a database.

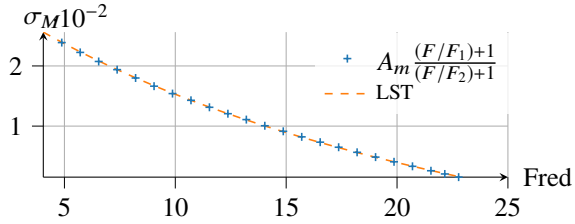

Figure 4: σ_M interpolation

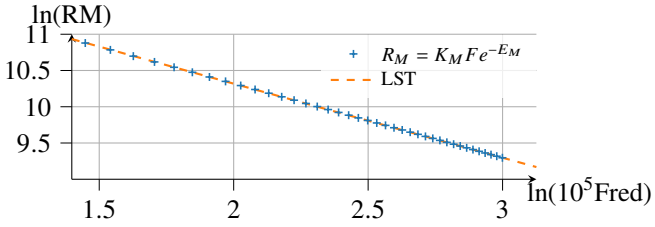

Figure 5: R_M interpolation

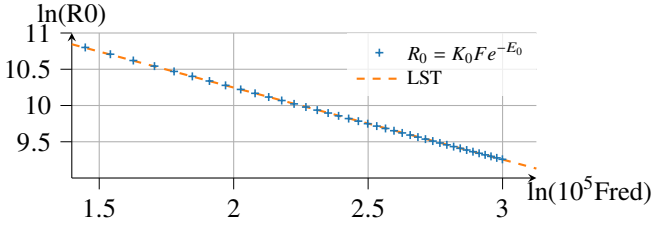

Figure 6: R_0 interpolation

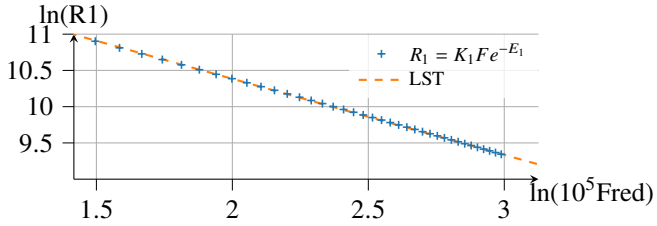

Figure 7: R_1 interpolation

Equations of interpolations of R_0, R_M, $\tilde{R}$, R_1, and σ_M evolution with reduced frequency F are expressed as

$$\sigma_M = A_m \frac{\frac{\mathrm{F}}{F_1} + 1}{\frac{\mathrm{F}}{F_2} + 1} \tag{11}$$

$$R_M = K_M \left(10^5 \ \mathrm{F}\right)^{E_M} \tag{12}$$

$$R_0 = K_0 \left(10^5 \ \mathrm{F}\right)^{E_0} \tag{13}$$

$$R_1 = K_1 \left(10^5 \ \mathrm{F}\right)^{E_1} \tag{14}$$

$$\tilde{R} = K_{\tilde{R}} \left(10^5 \ \mathrm{F}\right)^{E_{\tilde{R}}} \tag{15}$$

The linear correction is defined by

$$\frac{\sigma}{\sigma_M} = \left(Re_{\delta_1} - R_1\right) \frac{\tilde{K}}{\tilde{R} - R_1} \tag{16}$$

where

$$\tilde{K} = \frac{2\left(R_1 - \tilde{R}\right)}{2R_1 - \tilde{R} - R_M} \tag{17}$$

The parabolas method is used together with the e^N-method which computes the amplification factor N of an instability, for a given reduced frequency F. To confront the concept of this new model with LST results, a dedicated database has been embedded in ONERA's elsA software - along with the NSP model for the integration of amplification rates - and applied to a sharp cone at Mach 8 at zero angle of attack.

III. Application of Embedded Parabolas method in RANS solver

A. Cone Geometry and Free-stream Conditions

The free-stream conditions and geometry are adapted from Stetson et al. [32], which has been reproduced by Malik et al. [33], Kufner et al. [34], and Rosenboom et al. [35]. The geometry is a 7° half-angle ideally sharp cone at zero angle-of-attack. The gas is considered ideal. The free-stream conditions are as follows: the free-stream Mach number is set to $\mathrm{M}_\infty = 8.0$, the free-stream unit Reynolds number to $\mathrm{Re}_\infty = 8.202 \times 10^6$ 1/m, and the free-stream stagnation temperature to $\mathrm{Ti}_\infty = 750$K which corresponds to a free-stream static temperature of $\mathrm{T}_\infty = 54.35$K. Schneider [36] specifies that the free-stream Reynolds number used by Rosenboom was computed from the free-stream stagnation pressure $\mathrm{Pi}_\infty = 4.0$MPa by using the Mack-modified form of Sutherland's viscosity law. If normal Sutherland's viscosity law was used, the result would have been $\mathrm{Re}_\infty = 8.76 \times 10^6$ 1/m, which makes and error about 7%. In his experiment, Stetson had a one-meter-long cone, whereas in the simulations of Rosenboom and Kufner a two-meters-long one was used.

B. Grid Distribution and Numerical Methods

The grid distribution is shown in Figure 8 with the Mach number contour to show the control line following the shock layer. The flow is resolved with 600 points in the freestream direction and 400 points in the wall-normal direction, between the surface and the control line. Grid clustering is applied in the boundary-layer and the shock layer. The grid is composed of 290,000 points in total. The laminar mean flow is computed with ONERA's elsA software using a Roe scheme with Van Albada limiter for space discretization and backward Euler scheme for time integration, with scalar LU-SSOR scheme for implicit time integration. A CFL slope from 0.01 to 10 is used over the 10,000 first iterations and fixed at 10 afterward. The size of the first grid cell is adapted so that the size of the cell at the boundary-layer edge is less than 10% of δ, along with a grid expansion ratio inside the boundary layer set to 1.04 in the wall-normal direction. The simulation is stopped when the boundary-layer profiles are considered to have reached a converged state.

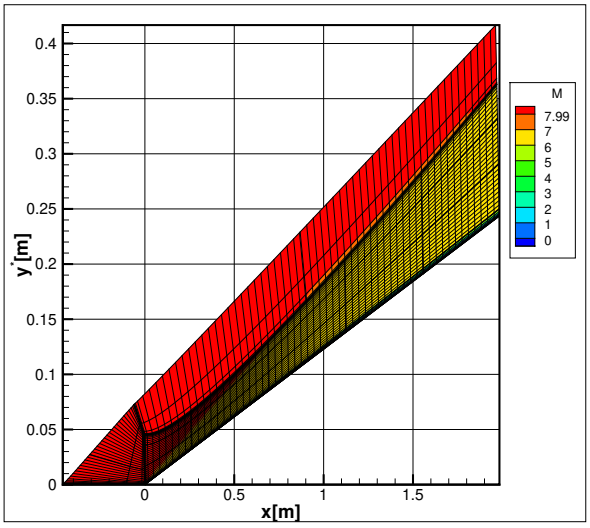

Figure 8: Numerical grid: 1 point over 10 is shown Scaling is different in x and y directions

C. Mean-Flow Computation

The mean flow is computed over an adiabatic wall and the accuracy of the simulation is checked by comparing the results with Rosenboom's ones on mean-flow profiles at stations $s \in [0.1, 0.5, 0.9]$ (Figures 9 and 10), boundary-layer thickness and pressure gradient evolution along the cone arclength s (Figures 11 and 12). Three different boundary-layer thicknesses (δ_u, δ_t, δ_h) were plotted by Rosenboom: they have been computed respectively from velocity (dynamic boundary-layer), temperature (thermal boundary-layer) and total enthalpy (total enthalpy boundary-layer). For enthalpy, the boundary-layer is defined as the wall-normal distance were 99.9% of the total enthalpy of the free stream. In Figure 12 , the pressure gradient is very important at the leading-edge and decreases downstream: the fluid is accelerated until roughly half the cone.

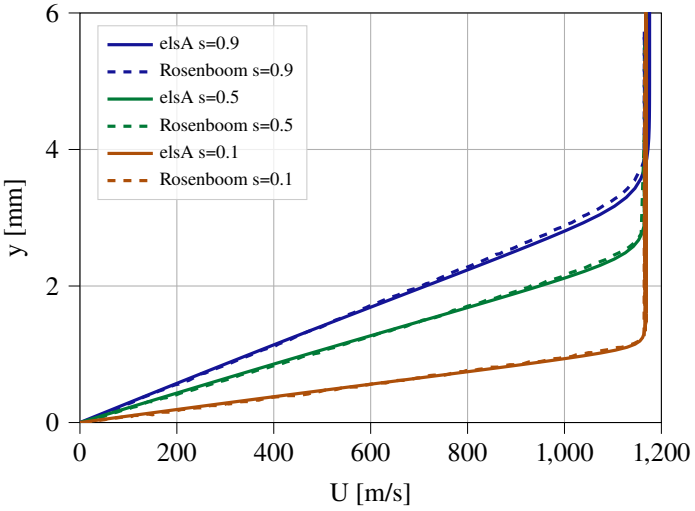

Figure 9: Comparison of velocity profiles along wall-normal coordinate at stations s = 0.1, 0.5 **and** 0.9

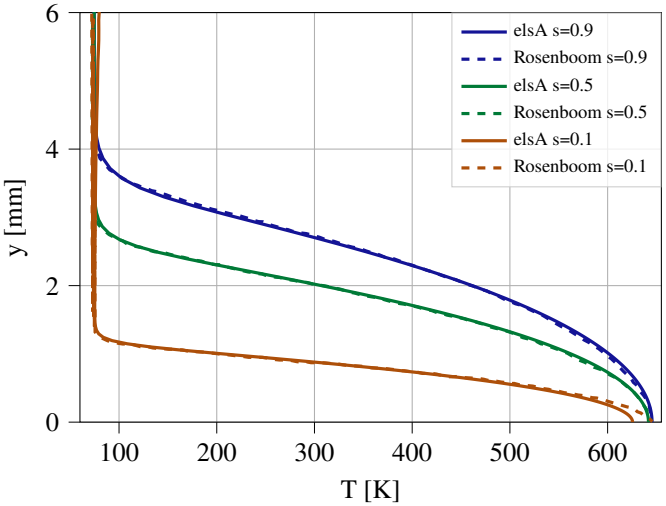

Figure 10: Comparison of temperature profiles along wall-normal coordinate at stations s = 0.1, 0.5 **and** 0.9

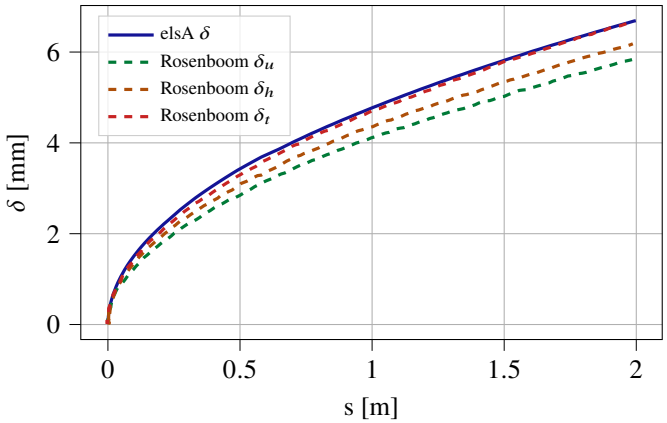

Figure 11: Comparison of boundary-layer thickness evolution along the cone arclength

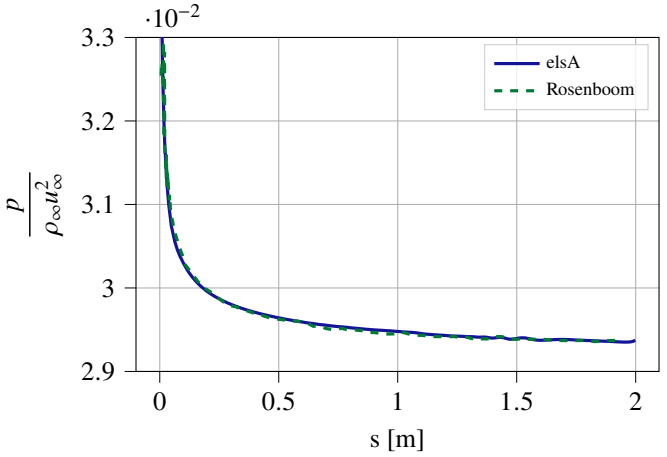

Figure 12: Comparison of pressure gradient evolution along the cone arclength

D. Local Linear Stability results comparison

Stability results for the second mode are first compared against those of Rosenboom. In Figure 13 , the current code computes the same evolution of the amplification rates as Rosenboom's except for the end of each parabolas: the 2nd branch of the second mode goes faster toward zero for the current stability code. It has an impact on the amplification factor maximum of each frequency as shown in Figure 14 . Although, these maxima are not the same between the two stability codes, the limit defined by the critical N-factor N_{tr} is usually crossed before this maxima, where the two stability codes give amplification rates with negligible error.

Higher unstable frequencies are located near the cone leading edge. In this region, the growth rates of the two stability codes are quite different: as plotted in Figure 13, the relative error on the maximum value for frequency 400kHz is about 20%.This could be a critical issue if the transition was to occur here. However, the N-factors are considered low enough to not trigger transition, which is

supported by experimental results. Indeed, Stetson et al. [32] noticed that the boundary-layer starts transitioning around s = 0.57. Rosenboom deduced from this result that the transition is triggered by the frequency 180kHz. The associated critical N-factor is deduced at $N_{tr} \approx 4.5$. Using the same critical N-factor N_{tr}, the stability code used presently predicts a transition triggered by the frequency 175kHz - which makes an error about 3% - and the transition location is found at s = 0.59. The relative error on the transition location between the two codes is about 3%.

These differences between both results can come from mainly two factors. The equations of the current stability code are made dimensionless using boundary-layer quantities and variables at boundary-layer edge. Although the two numerical simulations compute the same mean flow, extracting boundary-layer quantities to compute flow stability requires the determination of the boundary-layer edge. However this velocity is not constant, making this determination tricky. Another explanation is linked to the stability code itself: Malik [37] showed that the choice of the scheme for the discretization of the stability equation can have an impact on the growth rate value. However, references in Rosenboom's paper could not give any further information on the stability code. In any case, the current stability code is aimed to be used for the modelization of the second mode growth rate, thus this differences are considered low enough to have negligible impact on the final modelization.

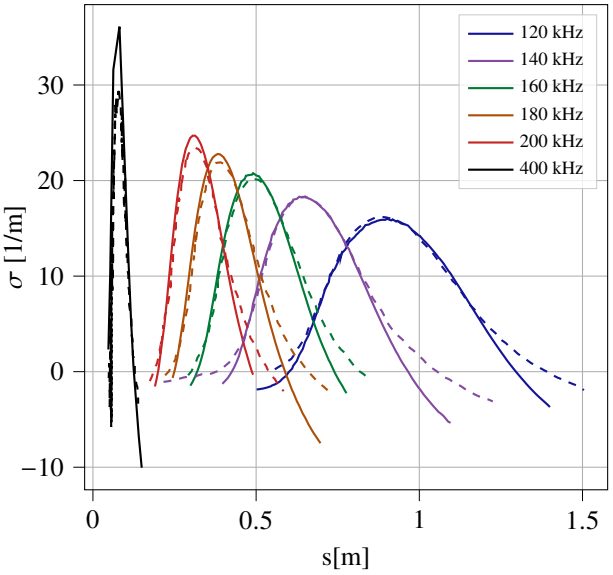

Figure 13: Comparison of growth rate of linear local stability code (plain) and Rosenboom's (dashed), for several frequencies propagating along the cone surface

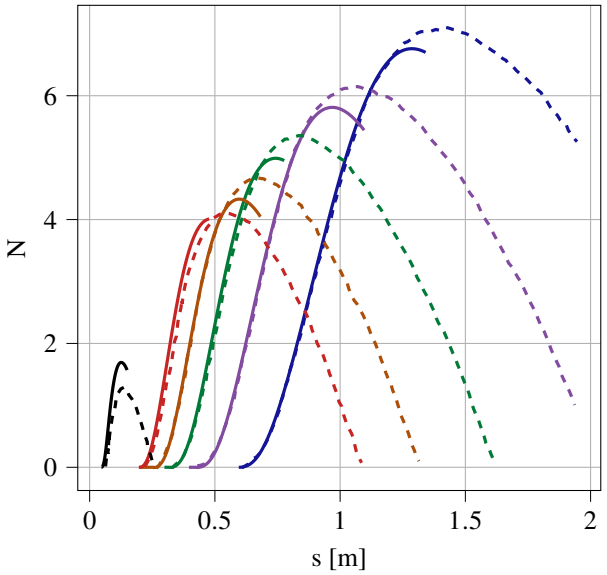

Figure 14: Comparison of N-factors from current linear local stability code (plain) and Rosenboom's (dashed) for several frequencies, same legend as in Figure 13

E. Transition prediction with parabolas method

The local linear stability code presented in the previous subsection has been used for the construction of the current database. The comparisation of amplification rate evolutions and N-factors for several frequencies with both methods are presented respectively in Figures 15 and 16 to assess the error of the model.

The amplification rates computed from elsA's parabolas method allow to find the same evolution of amplification rates as the LST. For low frequencies, the evolution differs slightly between the two methods, which impacts the maxima of N-factors. As said in the previous subsection, the limit defined by the critical amplification factor N_{tr} is usually crossed before the maximum. Thus, the error of the reconstructed parabolas for low frequencies is considered negligible.

Figure 16 shows the comparison of N-factors between LST and embedded method in elsA. The integration of amplification rates is recasted into a transport equation, using Bégou's method.

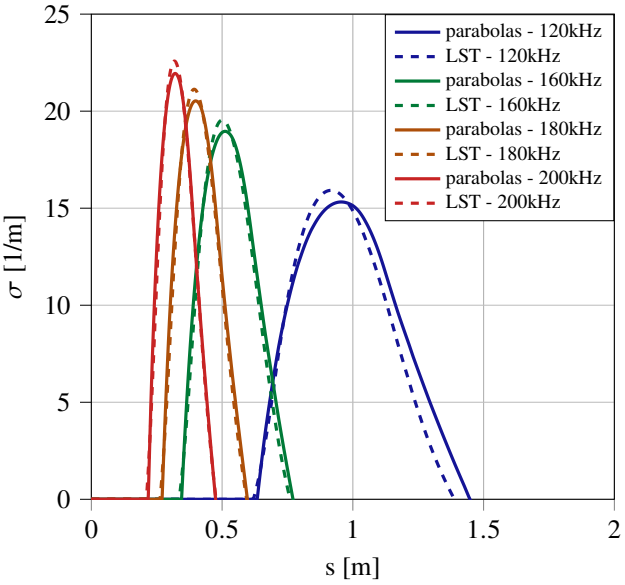

Figure 15: Comparison of growth rate from elsA (plain) and LST's (dashed) for several frequencies

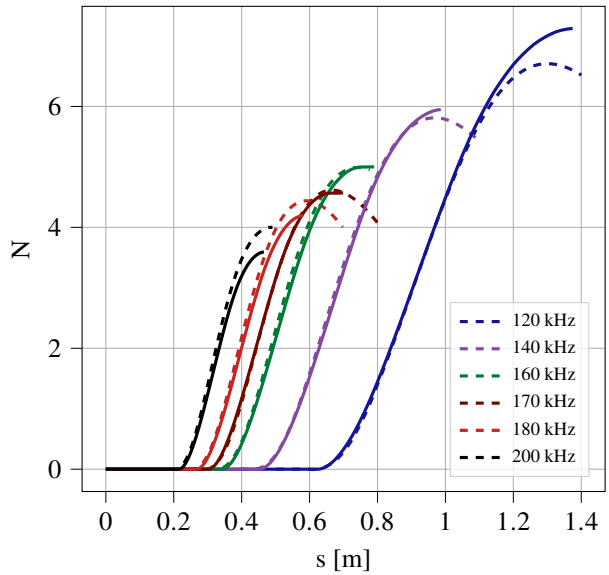

Figure 16: Comparison of N-factors from elsA (plain) and LST's (dashed) of the cone for several frequencies

The N-factors evolutions computed from elsA's parabolas method matches that of the LST for the cone, except for the maxima of low and high frequencies. These discrepancies are the same as the ones for the construction of the model: reconstruction of the LST by the parabolas method at low frequencies is not yet accurate enough to match the second branch. Even tough, at s = 0.59, the transition is triggered by a frequency between 170 and 180 kHz, and the associated N_t is about 4.5 which is the same results as LST one.

IV. Conclusion

The parabolas method has been extended with a new model for Mack's mode in order to predict natural laminar-turbulent transition for hypersonic flows. This model has been applied to a sharp cone geometry at Mach number 8 following the experiment of Stetson, and has proven its capability to reproduce the amplification rate evolution predicted by the LST. This method, when coupled with the e^N-method, is able to give the beginning of the transitional region for RANS code at smaller computational costs and in good agreement with LST results. Moreover, it allows engineers to easily compute transition location because using this method bypasses the resolution of stability equations. This new model still needs to be enriched with isothermal profiles and wider pressure gradient range in order to be used on more complex geometries for hypersonic applications.

References

[1] Reshotko, E., "Boundary Layer Instability, Transition and Control," *32nd Aerospace Sciences Meeting and Exhibit*, American Institute of Aeronautics and Astronautics, 1994. https://doi.org/10.2514/6.1994-1.

[2] Mack, L. M., "Boundary-Layer Linear Stability Theory," Tech. rep., California Inst of Tech Pasadena Jet Propulsion Lab, 1984.

[3] Fuller, R., Saunders, W., Vandsburger, U., Fuller, R., Saunders, W., and Vandsburger, U., "Neural Network Estimation of Disturbance Growth Using a Linear Stability Numerical Model," *35th Aerospace Sciences Meeting and Exhibit*, American Institute of Aeronautics and Astronautics, 1997. https://doi.org/10.2514/6.1997-559.

[4] Arnal, D., "Transition Prediction in Transonic Flow," *Symposium Transsonicum III*, edited by J. Zierep and H. Oertel, Springer, Berlin, Heidelberg, 1989, pp. 253–262. https://doi.org/10.1007/978-3-642-83584-1_21.

[5] Van Ingen, J., "A Suggested Semi-Empirical Method for the Calculation of the Boundary Layer Transition Region," Tech. rep., Delft University of Technology, 1956.

[6] Smith, A. M. O., and Gamberoni, N., "Transition, Pressure Gradient and Stability Theory," Rapport Technique ES 26 388, Douglas Aircraft Company, El Segundo Division, El Segundo, Calif, 1956.

[7] Arnal, D., "Description and Prediction of Transition in Two-Dimensional, Incompressible Flow," AGARD Report R-709, Special Course on Stability and Transition of Laminar Flows, 1984.

[8] Arnal, D., Houdeville, R., Seraudie, A., and Vermeersch, O., "Overview of Laminar-Turbulent Transition Investigations at ONERA Toulouse," *41st AIAA Fluid Dynamics Conference and Exhibit*, American Institute of Aeronautics and Astronautics, 2011. https://doi.org/10.2514/6.2011-3074.

[9] Drela, M., and Giles, M. B., "Viscous-Inviscid Analysis of Transonic and Low Reynolds Number Airfoils," *AIAA Journal*, Vol. 25, No. 10, 1987, pp. 1347–1355. https://doi.org/10.2514/3.9789.

[10] Menter, F. R., Langtry, R. B., Likki, S. R., Suzen, Y. B., Huang, P. G., and Völker, S., "A Correlation-Based Transition Model Using Local Variables—Part I: Model Formulation," *Journal of Turbomachinery*, Vol. 128, No. 3, 2004, pp. 413–422. https://doi.org/10.1115/1.2184352.

[11] Frauholz, S., Reinartz, B. U., Müller, S., and Behr, M., "Transition Prediction for Scramjets Using γ-$Re_{\theta t}$ Model Coupled to Two Turbulence Models," *Journal of Propulsion and Power*, Vol. 31, No. 5, 2015, pp. 1404–1422. https://doi.org/10.2514/1.B35630.

[12] Wang, Y., Li, Y., Xiao, L., Zhang, B., and Li, Y., "Similarity-Solution-Based Improvement of γ-$Re_{\theta t}$ Model for Hypersonic Transition Prediction," *International Journal of Heat and Mass Transfer*, Vol. 124, 2018, pp. 491–503. https://doi.org/10.1016/j.ijheatmasstransfer.2018.03.092.

[13] Walters, D. K., and Leylek, J. H., "Computational Fluid Dynamics Study of Wake-Induced Transition on a Compressor-Like Flat Plate," *Journal of Turbomachinery*, Vol. 127, No. 1, 2005, pp. 52–63. https://doi.org/10.1115/1.1791650.

[14] Warren, E. S., and Hassan, H. A., "Transition Closure Model for Predicting Transition Onset," *Journal of Aircraft*, Vol. 35, No. 5, 1998, pp. 769–775. https://doi.org/10.2514/2.2368.

[15] Xu, J., Bai, J., Qiao, L., Zhang, Y., and Fu, Z., "Fully Local Formulation of a Transition Closure Model for Transitional Flow Simulations," *AIAA Journal*, Vol. 54, No. 10, 2016, pp. 3015–3023. https://doi.org/10.2514/1.J054808.

[16] Papp, J. L., and Dash, S. M., "Rapid Engineering Approach to Modeling Hypersonic Laminar-To-Turbulent Transitional Flows," *Journal of Spacecraft and Rockets*, Vol. 42, No. 3, 2005, pp. 467–475. https://doi.org/10.2514/1.1854.

[17] Xu, J., Bai, J., Fu, Z., Qiao, L., Zhang, Y., and Xu, J., "Parallel Compatible Transition Closure Model for High-Speed Transitional Flow," *AIAA Journal*, Vol. 55, No. 9, 2017, pp. 3040–3050. https://doi.org/10.2514/1.J055711.

[18] Wang, L., and Fu, S., "Modelling Flow Transition in a Hypersonic Boundary-Layer with Reynolds-Averaged Navier-Stokes Approach," *Science in China Series G: Physics, Mechanics and Astronomy*, Vol. 52, No. 5, 2009, pp. 768–774. https://doi.org/10.1007/s11433-009-0047-8.

[19] Wang, L., and Fu, S., "Development of an Intermittency Equation for the Modeling of the Supersonic/Hypersonic Boundary Layer Flow Transition," *Flow, Turbulence and Combustion*, Vol. 87, No. 1, 2011, pp. 165–187. https://doi.org/10.1007/s10494-011-9336-1.

[20] Zhou, L., Yan, C., Hao, Z. H., and Du, R. F., "Improved k–ω–γ Model for Hypersonic Boundary Layer Transition Prediction," *International Journal of Heat and Mass Transfer*, Vol. 94, 2016, pp. 380–389. https://doi.org/10.1016/j.ijheatmasstransfer.2015.11.048.

[21] Zhou, L., Li, R., Hao, Z., Zaripov, D. I., and Yan, C., "Improved K-ω-γ Model for Crossflow-Induced Transition Prediction in Hypersonic Flow," *International Journal of Heat and Mass Transfer*, Vol. 115, 2017, pp. 115–130. https://doi.org/10.1016/j.ijheatmasstransfer.2017.08.013.

[22] Zhou, L., Zhao, R., and Li, R., "A Combined Criteria-Based Method for Hypersonic Three-Dimensional Boundary Layer Transition Prediction," *Aerospace Science and Technology*, Vol. 73, 2018, pp. 105–117. https://doi.org/10.1016/j.ast.2017.12.002.

[23] Fu, S., and Wang, L., "RANS Modeling of High-Speed Aerodynamic Flow Transition with Consideration of Stability Theory," *Progress in Aerospace Sciences*, Vol. 58, 2013, pp. 36–59. https://doi.org/10.1016/j.paerosci.2012.08.004.

[24] Van Ingen, J., "The eN Method for Transition Prediction. Historical Review of Work at TU Delft," *38th Fluid Dynamics Conference and Exhibit*, American Institute of Aeronautics and Astronautics, 2008. https://doi.org/10.2514/6.2008-3830.

[25] Drela, M., "Implicit Implementation of the Full e^N Transition Criterion," *21st AIAA Applied Aerodynamics Conference*, American Institute of Aeronautics and Astronautics, 2003. https://doi.org/10.2514/6.2003-4066.

[26] Crouch, J. D., Crouch, I. W. M., and Ng, L. L., "Transition Prediction for Three-Dimensional Boundary Layers in Computational Fluid Dynamics Applications," *AIAA Journal*, Vol. 40, No. 8, 2002, pp. 1536–1541. https://doi.org/10.2514/2.1850.

[27] Danvin, F., Olazabal, M., and Pinna, F., "Laminar to Turbulent Transition Prediction in Hypersonic Flows with Neural Networks Committee," *AIAA Aviation 2019 Forum*, AIAA AVIATION Forum, American Institute of Aeronautics and Astronautics, 2019. https://doi.org/10.2514/6.2019-2837.

[28] Bégou, G., Deniau, H., Vermeersch, O., and Casalis, G., "Database Approach for Laminar-Turbulent Transition Prediction: Navier–Stokes Compatible Reformulation," *AIAA Journal*, Vol. 55, No. 11, 2017, pp. 3648–3660. https://doi.org/10.2514/1.J056018.

[29] Orszag, S. A., "Accurate Solution of the Orr–Sommerfeld Stability Equation," *Journal of Fluid Mechanics*, Vol. 50, No. 4, 1971, pp. 689–703. https://doi.org/10.1017/S0022112071002842.

[30] Schmid, P. J., and Henningson, D. S., *Stability and Transition in Shear Flows*, Applied Mathematical Sciences, Springer-Verlag, New York, 2001. https://doi.org/10.1007/978-1-4613-0185-1.

[31] Lees, L., and Lin, C. C., "Investigation of the Stability of the Laminar Boundary Layer in a Compressible Fluid," 1946.

[32] Stetson, K. J., Thompson, E. R., Donaldson, J. C., and Siler, L. G., "Laminar Boundary Layer Stability Experiments on a Cone at Mach 8. II- Blunt Cone," *22nd Aerospace Sciences Meeting*, American Institute of Aeronautics and Astronautics, 1984. https://doi.org/10.2514/6.1984-6.

[33] Malik, M., Spall, R., and Chang, C.-L., "Effect of Nose Bluntness on Boundary Layer Stability and Transition," *28th Aerospace Sciences Meeting*, American Institute of Aeronautics and Astronautics, 1990. https://doi.org/10.2514/6.1990-112.

[34] Kufner, E., Dallmann, U., and Stilla, J., "Instability of Hypersonic Flow Past Blunt Cones - Effects of Mean Flow Variations," *23rd Fluid Dynamics, Plasmadynamics, and Lasers Conference*, American Institute of Aeronautics and Astronautics, 1993. https://doi.org/10.2514/6.1993-2983.

[35] Rosenboom, I., Hein, S., and Dallmann, U., "Influence of Nose Bluntness on Boundary-Layer Instabilities in Hypersonic Cone Flows," *30th Fluid Dynamics Conference*, American Institute of Aeronautics and Astronautics, 1999. https://doi.org/10.2514/6.1999-3591.

[36] Schneider, S. P., "Hypersonic Laminar–Turbulent Transition on Circular Cones and Scramjet Forebodies," *Progress in Aerospace Sciences*, Vol. 40, No. 1, 2004, pp. 1–50. https://doi.org/10.1016/j.paerosci.2003.11.001.

[37] Malik, M. R., "Numerical Methods for Hypersonic Boundary Layer Stability," *Journal of Computational Physics*, Vol. 86, No. 2, 1990, pp. 376–413. https://doi.org/10.1016/0021-9991(90)90106-B.